Scripta Materialia 146 (2018) 335–339

Contents lists available at ScienceDirect

Scripta Materialia

journal homepage: www.elsevier.com/locate/scriptamat

Regular article

The effect of helium implantation on the deformation behaviour of tungsten: X-ray micro-diffraction and nanoindentation

S. Das [a], D.E.J. Armstrong [b], Y. Zayachuk [b], W. Liu [c], R. Xu [c], F. Hofmann [a,*]

[a] Department of Engineering Science, University of Oxford, Parks Road, Oxford OX1 3PJ, UK
[b] Department of Materials, University of Oxford, Parks Road, Oxford OX1 3PH, UK
[c] Advanced Photon Source, Argonne National Lab, 9700 South Cass Avenue, Argonne, IL 60439, USA

ARTICLE INFO

Article history:
Received 7 August 2017
Received in revised form 11 December 2017
Accepted 12 December 2017
Available online xxxx

Keywords:
Nanoindentation
Laue micro-diffraction
Ion implantation damage
Fusion armour materials

ABSTRACT

The effect of helium-implantation-induced defects on deformation behaviour is examined by comparing spherical nano-indents in unimplanted and helium-implanted regions of a tungsten single crystal. Helium-implantation increases hardness and causes large pileups. 3D-resolved X-ray micro-diffraction uniquely allows examination of the complex lattice distortions beneath specific indents. In the ion-implanted material we find reduced lattice rotations and residual strains due to indentation, indicating a more confined plastic zone. Together, our observations suggest that helium-induced defects initially act as efficient obstacles to dislocation motion, but are weakened by the subsequent passage of dislocations, causing a reduction in work hardening capacity.

Tungsten is a promising candidate material for plasma facing components in future fusion reactors due to its high melting point, its strength at high temperatures and low sputtering yield [1–3]. However, challenges arise from its low fracture toughness, high brittle to ductile transition temperature (BDTT) [4] and poor machinability.

In the fusion reactor environment, armour components will be exposed to high temperatures (>900 °C) and bombardment with high-energy fusion neutrons (14.1 MeV) [3]. Interaction of these energetic neutrons with the tungsten lattice leads to collision cascades and the subsequent formation of defects in the material [5]. Furthermore, it causes transmutation, resulting in the formation of rhenium, osmium and tantalum, as well as hydrogen (H) and helium (He) [6–7]. At the anticipated operating temperatures, interstitial mobility of these gasses is high, allowing them to diffuse to defects, cracks or grain boundaries, resulting in embrittlement and hardening [8]. Hydrogen and helium will also be introduced into the material at plasma-facing surfaces exposed to large fluences of both elements [9–10].

The defect microstructure in tungsten is heavily influenced by the strong binding of helium to vacancies [11]. Previously nano-indentation showed a substantial increase in the hardness of tungsten after helium-ion implantation [12]. Interestingly helium ion implantation had a much greater effect on hardness than collision cascade damage caused by self-ion bombardment. This suggests that the presence of helium enhances defect retention and/or increases obstacle strength [12].

The effect of helium implantation on the mechanical properties of tungsten is potentially life limiting for the divertor, with significant economic consequences for fusion power. Resolving this problem requires a clear picture of the mechanisms governing the interaction of implantation defects with dislocation-mediated inelastic deformation. Experimentally these interactions are challenging to probe and at present remain poorly understood.

In this study, we consider spherical nano-indents in helium-implanted and unimplanted regions of the same tungsten single crystal, enabling a direct comparison and ensuring that any observed changes between the two regions are solely due to helium-implantation-induced defects. Using synchrotron X-ray micro-diffraction we are able to probe the lattice rotations and residual lattice strains beneath specific indents. These measurements uniquely provide access to the full, complex 3D lattice distortion field, whereas FIB lift-out and SEM/TEM observations, for example, only capture one slice though the indent. Importantly, since these X-ray measurements are non-destructive, the residual stress state remains unaltered. This 3D information is essential to unambiguously assess the underlying deformation fields that lead to the changes in surface morphology examinable by AFM or SEM (see exemplary finite element simulation in Supplementary section). Our results reveal striking differences that are discussed in terms of the interaction between helium-induced defects and dislocations.

A 5 mm diameter, 0.8 mm thick disk with [001] out-of-plane orientation was cut from a tungsten single crystal (99.99% purity). The [001] surface was mechanically ground and then polished using diamond

* Corresponding author.
E-mail address: felix.hofmann@eng.ox.ac.uk (F. Hofmann).

https://doi.org/10.1016/j.scriptamat.2017.12.014
1359-6462/

paste. A final chemo-mechanical polishing step with 0.1 μm colloidal silica suspension produced a high quality surface finish.

Part of the sample was implanted with helium ions at 298 K using a 2 MeV ion accelerator at the National Ion Beam Centre, University of Surrey, UK. Implantation was carried out at room temperature (298 K) and using a raster scanned beam to ensure a uniform implantation dose. A combination of different ion energies and fluences was used to obtain a near uniform helium ion concentration in excess of 3000 appm within a ~2.8 μm thick implanted layer [8,13–14]. Fig. 1(a) shows the implantation profile estimated using the SRIM code [15] (displacement energy of 68 eV, single-layer calculation model [16]). Between 0 and 2.8 μm depth, a helium ion concentration of ~3110 ± 270 appm is obtained with an associated damage of 0.24 ± 0.02 displacements per atom (dpa). Recoils induced by helium implantation have predominantly low energy, suggesting Frenkel pair formation as the main damage mechanism [14]. Since vacancy mobility is low at room temperature little defect clustering is expected [12,17–19].

Nanoindentation was performed using an MTS NanoXp with a spherical, ~4.2 μm radius diamond indenter tip. Indents were made to a maximum displacement of 500 nm with a 50 μm spacing between indents. Use of a spherical, axis-symmetric indenter removes the additional complexity, associated with in-plane indenter orientation relative to the crystal, found in Berkovich indentation. Fig. 1(b) shows the load-displacement curves of the two indents considered in more detail below.

The load displacement curves show an initial Hertzian elastic response that is almost identical in the unimplanted and implanted material. This is as expected since ion-implantation-induced changes in elastic modulus are small [14,20]. At ~25 nm depth, the unimplanted sample shows a large pop-in, indicative of dislocation nucleation in the initially relatively defect free material at the onset of plastic deformation [21]. In the implanted sample, there are no obvious pop-ins. This indicates an easier nucleation of initial dislocation loops due to the presence of helium-implantation-induced defects. At larger indentation depths the implanted sample shows a significantly greater indentation load than the unimplanted material, suggesting a substantial hardening due to helium-implantation-induced defects. This behaviour agrees well with previous Berkovich indentation of helium-implanted tungsten [12–13,22].

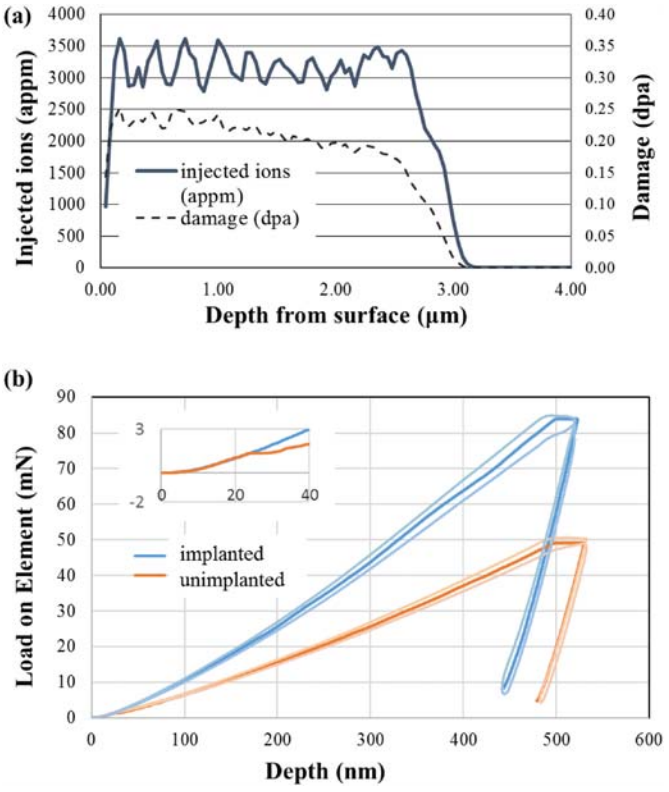

Fig. 1. (a) Profile of injected helium ion concentration calculated by SRIM (solid line) and the anticipated displacement damage (dashed line) plotted as a function of depth in the sample. (b) Load versus displacement curves for spherical indentation of the unimplanted and helium-implanted sample (faint lines = mean ± one standard deviation computed over 16 indents).

SEM micrographs of the nano-indents, recorded using a Zeiss Merlin FEG SEM, are shown in Fig. 2(a) and (b). Little pile up is present in the unimplanted sample. The implanted material, on the other hand, shows a much larger, localised pile up around the indent tip. A similar trend was observed by Beck et al. who reported a substantial increase in pile up around Berkovich indents in helium-implanted tungsten of unidentified orientation [22]. Unfortunately, in their work the relative contributions of ion-implantation defects and indentation geometry to this effect could not be distinguished. Interestingly, in our study, the effects of crystallography are clearly visible: The pileup shows a strong dependence on the in-plane crystal orientation. Along ⟨100⟩ directions the pileup is relatively small, whilst along ⟨110⟩ directions a larger pileup is present. This is very clear in the implanted sample, where, due to the orientation dependent large pile up, the indenter impression assumes a square shape (sides of the square are along the ⟨100⟩ direction). Such pile up patterns, localised in defined zones around the indent, and exhibiting a four-fold symmetry of out of plane displacement profile, have been previously observed in nano-indented (001) oriented Cu single crystals [23–24]. It can further be noted that the pileup in the implanted material shows a number of distinct steps indicated by small arrows in Fig. 2(b). This suggests a slip localisation, similar to the dislocation channel formation reported in irradiation-damaged fcc metals [25–26].

Micro-beam Laue diffraction measurements were carried out at beamline 34-ID-E, Advanced Photon Source, Argonne National Lab, USA. This instrument allows measurements of lattice orientation with sub-micron 3D resolution using the Differential Aperture X-ray Microscopy (DAXM) technique. A detailed description of the DAXM technique and the 34-ID-E instrument is provided elsewhere [27–29]. Here a polychromatic X-ray beam (5–30 keV), focussed to a size of ~500 nm, was used and measurements were carried out to a depth of 20 μm beneath the ion-implanted surface. Laue diffraction patterns contained 30+ peaks and were indexed and fitted using the LaueGo software package (J.Z. Tischler: tischler@anl.gov) to extract both lattice orientation and the full deviatoric lattice strain tensor at each measurement point in 3D space.

Lattice rotations, θ_x, θ_y and θ_z, due to nano-indentation, refer to changes in crystal orientation compared to the pristine (unimplanted and undeformed) single crystal. The right-handed coordinate frame used here, and the corresponding crystal directions, are shown in Fig. 2(a) and (b). Fig. 2(c) and (d) show lattice rotation maps about all three axes for indents in the unimplanted and implanted material respectively. These rotations are plotted on virtual YZ slices through the sample at three X positions (indicated by dashed yellow lines in Fig. 2(a) and (b)). Positions 1 and 3 correspond to slices 5 μm before and after the indent centre respectively, whilst position 2 corresponds to a slice through the indent centre.

In the unimplanted sample, lattice rotations are significantly larger than in the implanted material. However, both show similar patterns of lattice rotation variation at the different X positions (seen clearly in Fig. 4 in the Supplementary section). As expected θ_y is negative (anticlockwise rotation) before the indent centre (position 1) and positive after the indent centre (position 3). For θ_x a similar pattern is observed with a positive lobe to the right and a negative lobe to the left at positions 1 and 3. At the indent centre, rather than clear positive and negative lobes, a rapidly varying arrangement of lattice rotations is observed beneath the indent.